

Article

Graphene/Fe₃O₄ Nanocomposite as a Promising Material for Chemical Current Sources: A Theoretical Study

Vladislav V. Shunaev ^{1,*}  and Olga E. Glukhova ^{1,2} ¹ Department of Physics, Saratov State University, 410012 Saratov, Russia; glukhovaoe@sgu.ru² Institute for Bionic Technologies and Engineering, Sechenov University, 119991 Moscow, Russia

* Correspondence: shunaevvv@sgu.ru; Tel.: +7-8452-514562

Abstract: The outstanding mechanical and conductive properties of graphene and high theoretical capacity of magnetite make a composite based on these two structures a prospective material for application in flexible energy storage devices. In this study using quantum chemical methods, the influence of magnetite concentration on energetic and electronic parameters of graphene/Fe₃O₄ composites is estimated. It is found that the addition of magnetite to pure graphene significantly changes its zone structure and capacitive properties. By varying the concentration of Fe₃O₄ particles, it is possible to tune the capacity of the composite for application in hybrid and symmetric supercapacitors.

Keywords: graphene; iron oxide; modeling; quantum capacitance; zone structure



Citation: Shunaev, V.V.; Glukhova, O.E. Graphene/Fe₃O₄ Nanocomposite as a Promising Material for Chemical Current Sources: A Theoretical Study. *Membranes* **2021**, *11*, 642. <https://doi.org/10.3390/membranes11080642>

Academic Editors: Vladislav A. Sadykov and Dirk Henkensmeier

Received: 29 July 2021

Accepted: 19 August 2021

Published: 20 August 2021

Publisher's Note: MDPI stays neutral with regard to jurisdictional claims in published maps and institutional affiliations.



Copyright: © 2021 by the authors. Licensee MDPI, Basel, Switzerland. This article is an open access article distributed under the terms and conditions of the Creative Commons Attribution (CC BY) license (<https://creativecommons.org/licenses/by/4.0/>).

1. Introduction

Composites based on iron oxides and carbon nanomaterials have attracted increased attention from developers of flexible energy storage devices (lithium ion batteries and supercapacitors) [1–4]. One iron oxide, magnetite Fe₃O₄, is often used in materials synthesis due to its richness, ecological purity and high theoretical capacity (about 926 mA·h/g), which is almost three times higher than the capacity of graphite [5,6]. However, anodes based on this metal have low electrical conductivity and cannot maintain structural stability over a large number of charge/discharge cycles. Graphene, with its high mechanical strength and flexibility, prevents the destruction of iron oxide. In addition, the high conductivity of graphene provides this composite with high electrochemical performance.

One of the often-used G/Fe₃O₄ syntheses is deposition of magnetite particles into graphene oxide with subsequent removal of oxygen groups. The composite obtained in this way can be called reduced graphene oxide (rGO)/Fe₃O₄. Liu and Sung reported that their paper based on monodisperse Fe₃O₄ grown in situ on rGO sheets showed a high specific capacitance of 368 F/g at 1 A/g that remained at 245 F/g at 5 A/g after 1000 cycles, indicating its suitability as flexible anode material for supercapacitors [7]. Zhao et al. developed a novel strategy for the preparation of sandwich-structured rGO/Fe₃O₄ that achieved higher reversible capacity and better cycle/rate performance in comparison to bulk Fe₃O₄ [8]. Shi et al. showed that Fe₃O₄/rGO nanocomposites with mass ratio m(Fe₃O₄):m(rGO) = 2.8 delivered the highest specific capacitance of 480 F/g at a discharge current density of 5 A/g [9]. The assembled lithium ion capacitors based on Fe₃O₄, rGO and activated carbon demonstrated an outstanding energy density of 98.8 W·h/kg and power density of 3.4 kW/kg with 78.9% of capacity saved after 1000 charge/discharge cycles [10]. The rGO/Fe₃O₄ composites synthesized by a simple and effective low-temperature thermal annealing method exhibited an energy density of 120.0 W·h/kg, a great power density of 45.4 kW/kg (achieved at 60.5 W·h/kg) and reasonably good cycling stability, with 94.1% capacity retention after 1000 cycles and 81.4% after 10,000 cycles [11].

However, some are of the mind that decoration of graphene without oxygen-containing moieties is more attractive since oxygen functional groups increase the number of sp²-sp³

bonds that significantly reduce graphene's conductivity [12,13]—an important parameter for chemical power sources. Taufik and R Saleh reported on a hydrothermal method of G/Fe₃O₄ nanocomposite synthesis [14]. Nene et al. developed a simple method to synthesize G/Fe₃O₄ nanocomposites in which ascorbic acid reduces Fe(acac)₃ at a specific temperature in the presence of carboxylated graphene and ultrapure water [15]. Escusson et al. designed a negative electrode based on G/Fe₃O₄ obtained by ultrasonic irradiation of few-layer graphene and nanocrystalline Fe₃O₄ [16]. After optimization, the cell voltage equaled 1.4 V, maximal energy density 9.4 W·h/kg and maximal power density 41.1 k·W/kg. Gu and Zhu obtained G/Fe₃O₄ nanocomposites via a sequential freeze-drying of graphene and iron ion suspension and solvent thermal synthesis method [17]. The anode based on this nanocomposite demonstrated a high reversible capacity of ~1145 mA·h/g after 120 cycles at 100 mA/g and a remarkable rate capability of 650 at 0.5 A/g.

Attempts at G/Fe₃O₄ study by mathematical modeling methods should also be noted. Using the Vienna ab initio simulation package, it was shown that magnetic and electron properties in this composite are determined by different interfacial terminations between graphene and Fe₃O₄ [18]. DFT calculations performed using Gaussian distribution showed that the addition of magnetite to graphene increases its ionization potential, leading to the creation of new negatively charged active sites that are also ready for nucleophilic interactions [19]. Earlier authors using quantum–chemical methods showed that the growth of magnetite concentrations in the γ -Fe₂O₃/CNT (carbon nanotubes) film leads to increases in the amount of charge on CNT and composite quantum capacitance (QC)—one of the two total specific capacity components [20,21]. The critical review performed suggested that a similar effect could be achieved in G/Fe₃O₄ composites. The aim of the work is to analyze the energy and electronic characteristics of freestanding G/Fe₃O₄ membranes with different concentrations of magnetite that would expand our knowledge of the processes occurring in flexible energy storage with electrodes based on G/Fe₃O₄ composites. The objects of the study were 2D composites with mass ratios m(Fe₃O₄):m(G) = 1:9, 1:4, 3:7 and 1:1, since these concentrations can clearly demonstrate gradual changes in graphene capacitive properties with the addition of magnetite nanocomposites, and such composites can be synthesized in experiments [16,17,22].

2. Methods

The search for ground states, as well as the calculation of the studied object's zone structure, was performed by a self-consistent-charge density-functional tight-binding method (SCC DFTB) [23]. In terms of computational speed, the SCC DFTB method is comparable to traditional semi-empirical methods but provides accuracy comparable to ab initio calculations. The method is based on the second order decomposition of total Kohn–Sham energy by charge density. The matrix elements of the undisturbed Hamiltonian $H_{\mu\nu}^0$ are represented by the minimal basis of atomic orbitals, using two particle approximation. Since the main type of interaction between graphene and magnetite particles is the van der Waals interaction, in addition to the band structure energy E_{BS} , repulsive energy E_{rep} and charge fluctuation energy E_{SCC} , the term E_{dis} that describes dispersion energy by Lennard-Jones potential was added:

$$E_{tot} = E_{BS} + E_{rep} + E_{SCC} + E_{dis}. \quad (1)$$

The band energy E_{BS} is found by the formula:

$$E_{BS} = \sum_{i\mu\nu} c_{\mu}^i c_{\nu}^i H_{\mu\nu}^0, \quad (2)$$

where c_{μ}^i and c_{ν}^i are coefficients for the decomposition of the molecular orbital into atomic orbitals. The term E_{SCC} can be found as follows:

$$E_{\text{SCC}} = \frac{1}{2} \sum_{\alpha\beta} \gamma_{\alpha\beta} \Delta q_{\alpha} \Delta q_{\beta} \quad (3)$$

where Δq_{α} and Δq_{β} are fluctuations of atoms α and β , respectively; $\gamma_{\alpha\beta}$ is the function that exponentially decreases with increasing distance between the α and β atoms and directly depends on chemical hardness [24].

The basic set trans3d-0-1 was used to define the interaction between Fe, O and C atoms [25]. Optimization was performed at a temperature of 300 K with $8 \times 8 \times 1$ Monkhorst–Pack Brillion zone sampling.

The binding energy E_b between graphene and Fe_3O_4 was found by the formula:

$$E_b = E(\text{G} + \text{Fe}_3\text{O}_4) - E(\text{G}) - E(\text{Fe}_3\text{O}_4) \quad (4)$$

where $E(\text{G} + \text{Fe}_3\text{O}_4)$ is the energy of the formed composite, and $E(\text{G})$ and $E(\text{Fe}_3\text{O}_4)$ are the energies of isolated graphene and Fe_3O_4 particles, respectively.

Electron transfer between graphene and Fe_3O_4 nanoparticles was tracked by Mulliken population analysis [26], where the atom's charge was calculated by the formula:

$$Z = Z_A - \text{GAP}_A \quad (5)$$

where Z_A is atomic number in the periodic table and GAP_A is the sum of the gross orbital product over all orbitals belonging to atom A.

3. Results

The iron nanoparticle atomic structure had the cubic space group Fd3m as in [17]. The concentration of magnetite particles on the graphene surface was varied by the dimensions of graphene nanoparticles. Table 1 shows translation vectors L_x and L_y , bonding energy E_b , Fermi level E_f and relative value of transferred charge $\Delta q(\text{Fe}_3\text{O}_4)/n(\text{C})$ for G/ Fe_3O_4 supercells with different mass ratios. The G/ Fe_3O_4 atomic supercell composite with a 1:1 ratio after optimization by the SCC DFTB method is shown in Figure 1. The binding energies E_b of magnetite particles with graphene of different sizes calculated by Formula (1) are negative, indicating the energy benefit of the considered compounds. Binding energy is mainly contributed by changes in electronic and dispersion energies. With increases in supercell dimensions, the modulus of electronic energy rises, leading to increases in binding energy, while dispersion energy falls, which leads to decreases in binding energy. As can be seen from Table 1, the bond between the Fe_3O_4 particle and graphene is strongest at mass ratio 1:4 (−2.65 eV); at this ratio, the rise in electronic energy surpasses the decrease in dispersion energy. The weakest E_b is observed at 3:7 (−1.53 eV); at this ratio, the rise in electronic energy is lower than the decrease in dispersion energy.

Table 1. Translation vectors L_x and L_y , bonding energy E_b , Fermi level E_f and relative value of transferred charge $\Delta q(\text{Fe}_3\text{O}_4)/n(\text{C})$ for G/ Fe_3O_4 supercells with different mass ratios.

$m(\text{Fe}_3\text{O}_4):m(\text{G})$	$L_x, \text{\AA}$	$L_y, \text{\AA}$	E_b, eV	E_f, eV	$\Delta q(\text{Fe}_3\text{O}_4)/n(\text{C}), \text{me}$
1:9	62.41	59.63	−2.36	−4.42	1.15
1:4	37.44	38.34	−2.65	−4.27	3.23
3:7	32.45	29.80	−1.53	−4.02	4.29
1:1	24.96	21.31	−1.99	−3.78	7.10

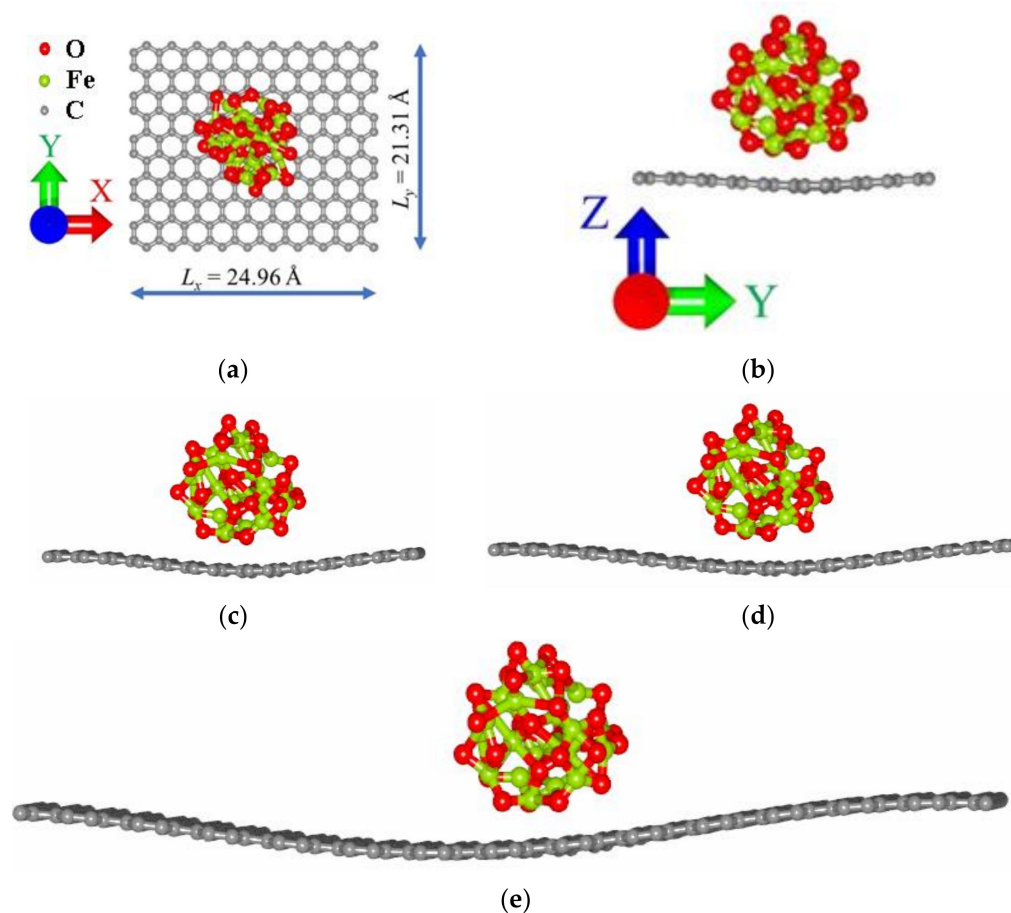


Figure 1. The atomic supercell of the membranes G/Fe₃O₄ after optimization by the SCC DFTB method, with mass ratios: (a) 1:1 top view; (b) 1:1 side view with translation vectors L_x and L_y; (c) 3:7 side view; (d) 1:4 side view; (e) 1:9 side view.

At the next stage, we calculated the activation energy—this is the energy that must be expended to start rapprochement between the components. For this purpose, we have constructed a graph of the dependence of dispersion energy $E'_{\text{dis}} = E_{\text{dis}} - E_{\text{dis}}^{\text{min}}$ on the distance between graphene and iron particles, where E_{dis} is the value of dispersion energy at the current mutual arrangement of objects, and $E_{\text{dis}}^{\text{min}}$ is the minimum value of dispersion energy in the considered interval from 0 to 2 Å (Figure 2). Herewith, the value 0 Å corresponds to the equilibrium distance between graphene and the Fe₃O₄ particle after optimization by the SCC DFTB method. The activation energy was assumed as the height of the resulting potential barrier, which must be overcome by a magnetite particle to attach to the graphene surface. As can be seen from Figure 2, the highest activation energy must be spent in the case of the minimum concentration of iron particles (1:9 (0.21 eV)), and the lowest in the case of 3:7 (0.07 eV). Note that the main part of the activation energy is spent on the curvature of the graphene sheet in the area of contact with the magnetite particle (Figure 1b). It is this mutual arrangement that provides the greatest binding energy.

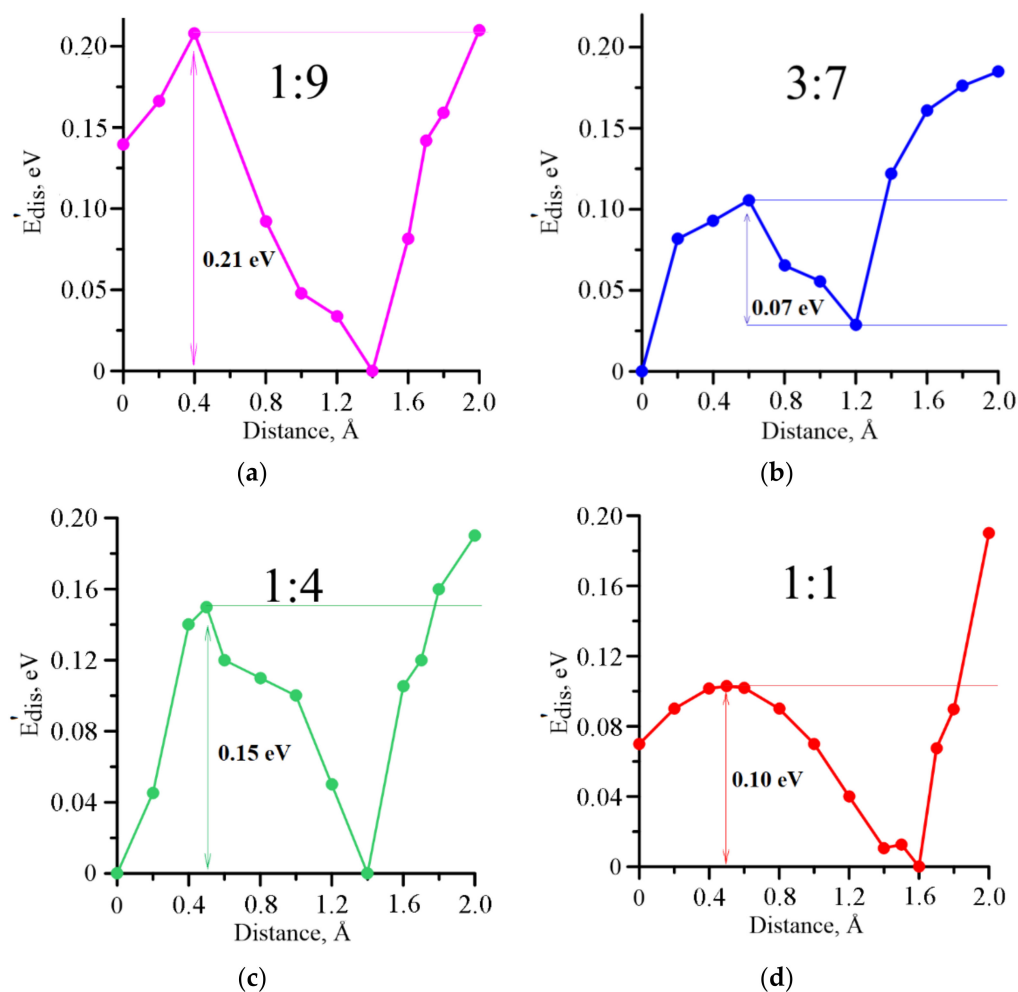


Figure 2. The dependence of dispersion energy on the distance between graphene and the Fe_3O_4 particle for different mass ratios of $m(\text{Fe}_3\text{O}_4):m(\text{G})$: (a) 1:9; (b) 3:7; (c) 1:4; (d) 1:1.

DOS curves for the considered structures are shown in Figure 3. It is notable that the doping of graphene with magnetite particles shifts the Fermi level to zero due to the presence of graphene oxide, as in the case of CNT doping with magnetite particles [21]. The value of the Fermi level for pure graphene is -4.68 eV; the values for $\text{G}/\text{Fe}_3\text{O}_4$ nanocomposites are shown in Table 1. It is seen that the DOS curve for pure graphene is close to zero at the Fermi level. The value of DOS rises with the growth of magnetite concentration and reaches maximum at the 1:1 ratio. In addition, it can be seen from the presented graph that at the mass ratio 1:9, the local minimum at the Fermi level as well as the symmetry-of-curve relative to the Fermi level line is observed, but that with a further increase in the concentration of magnetite, the local minimum and symmetry disappear; this indicates significant changes in the electronic properties of the material. The local maxima of DOS curves in the region of -6.8 to 2.0 eV are observed for all the considered supercells. In the region near -7 eV, the DOS values are located in the range from 0.46 eV^{-1} for 1:1 to 0.60 eV^{-1} for pure graphene; in the region near 2 eV, the DOS values are located in the range from 0.41 eV^{-1} for 1:4 to 1:9 to 0.42 eV^{-1} for 1:1. Note that after joining the graphene surface, the magnetite particles act as donors and transfer part of their charge to graphene, which becomes electronegative. The value of the total transferred charge varies between 1.41 and 1.74 e. However, the amount of charge per number of carbon atoms in graphene increases markedly with increases in the mass fraction of magnetite (Table 1).

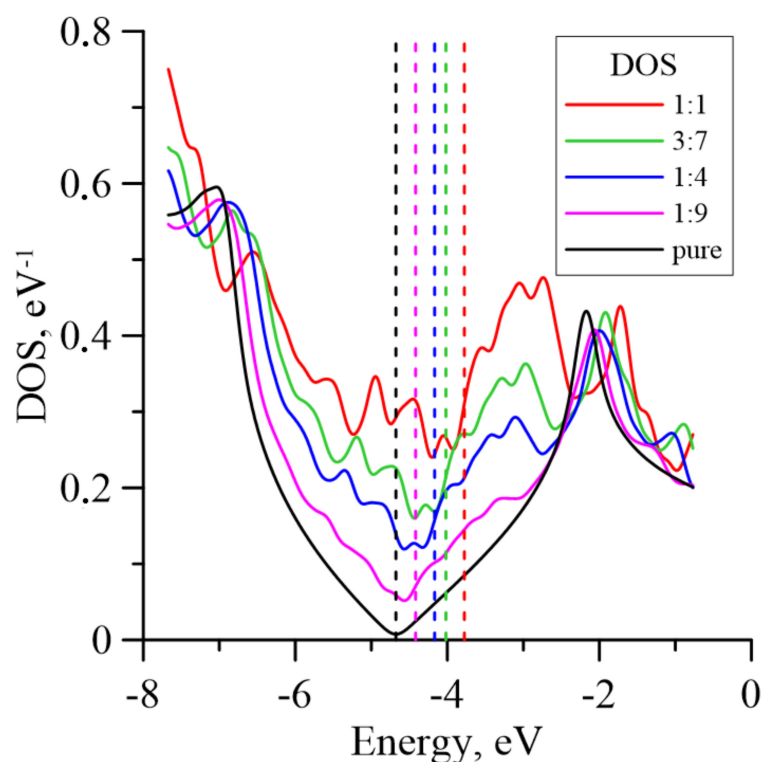


Figure 3. DOS curves for pure graphene and G/Fe₃O₄ membrane nanofilms with different concentrations of magnetite particles. The dotted lines correspond to Fermi levels.

Figure 4 shows the dependence of the QC on the voltages of pure graphene and graphene with different concentrations of Fe₃O₄ iron particles on its surface. As we can see, when the mass ratio of iron oxide to graphene is 1:9, the minimum QC shifts from 0 to -0.2 V, which is typical for graphene in the presence of various impurity defects [27–29]. A further increase in the concentration of iron oxide leads to a significant violation of the symmetry of the QC curve relative to the local minimum. An increase in the mass fraction of magnetite leads to a noticeable increase in the value of the QC at 0 V from 36.46 F/g for pure graphene to 583.52 F/g in the case of $m(\text{Fe}_3\text{O}_4):m(\text{G}) = 1:1$. This can be explained by significant increases in the relative charge q being transferred from magnetite to graphene.

The dotted lines in Figure 4 indicate the voltages corresponding to the stability limits of electrolyte systems with water (H₂O) and propylene carbonate (PC), which are often used in such systems as a solvent. The values of the QC at these boundaries relative to the values at 0 V $C_Q - C_Q(0)$ are presented in Table 2. This table allows us to estimate the contribution of the Faraday and non-Faraday components in the accumulated or given charge, depending on the applied voltage. For pure graphene, the Faraday component of the capacity, determined by QC, increases markedly when the voltage deviates from 0 V. For G/Fe₃O₄ nanocomposites, the Faraday component decreases when the reduction potential of H₂O is reached. Beneath the PC oxidation potential value, the QC changes take almost the same values for all the considered objects.

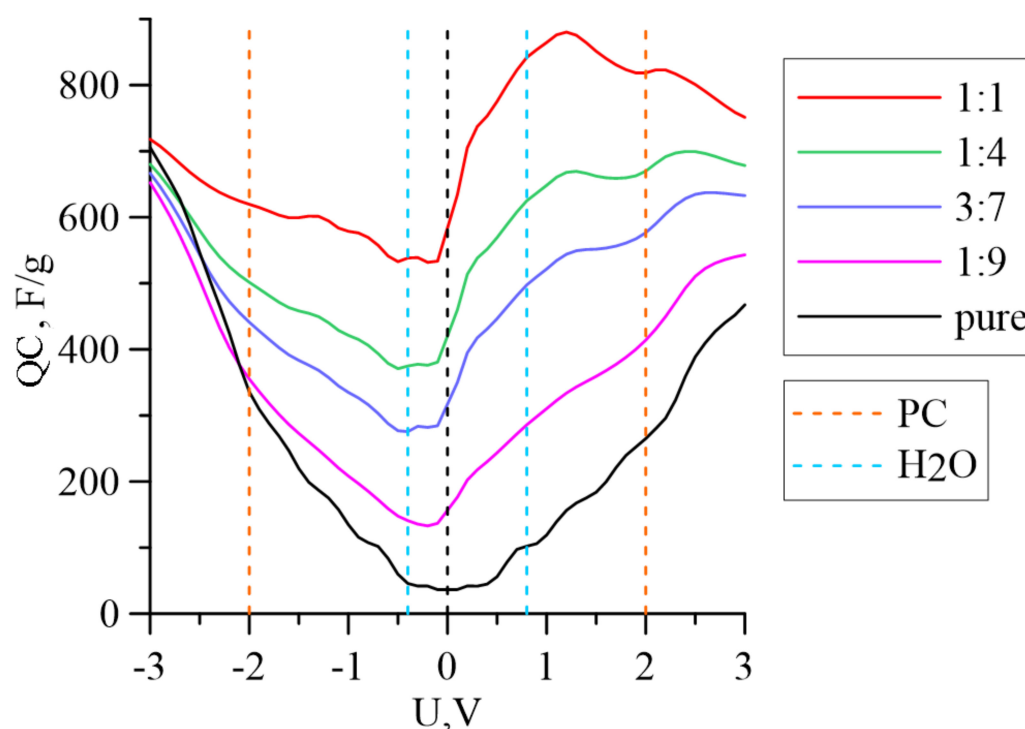


Figure 4. Dependence of QC for pure graphene and G/Fe₃O₄ membranes with different concentrations of magnetite particles on applied voltage. The black dotted line corresponds to 0 V.

Table 2. Values of QC for pure graphene and G/Fe₃O₄ membranes with different concentrations of magnetite particles at the stability limits of electrolyte systems with water and propylene carbonate relative to values at 0 V $C_Q-C_Q(0)$.

$m(\text{Fe}_3\text{O}_4):m(\text{G})$	−0.4 V (red. H ₂ O)	0.8 V (ox. H ₂ O)	−2.0 V (red. PC)	2.0 V (ox. PC)
Pure graphene	45.8	102.2	335.8	265.0
1:9	−15.8	129.2	198.6	257.3
1:4	−41.5	180.7	123.9	259.3
3:7	−45.6	204.6	81.1	249.4
1:1	−36.4	267.2	44.8	243.8

4. Conclusions

Using the SCC DFTB method, G/Fe₃O₄ atomic supercell composites were obtained with mass ratios $m(\text{Fe}_3\text{O}_4):m(\text{G}) = 1:9, 1:4, 3:7$ and $1:1$, observed during experimental synthesis. The energy characteristics of the studied objects indicate that the formation of 3:7 composites is the least energy-consuming, while the 1:4 compound is the most stable. These results can be used in experiments that receive G/Fe₃O₄ composites without preliminary treatment of GO—for example, by ultrasonic irradiation [16] or hydrothermal method [14]. Increases in the concentration of magnetite particles lead to significant changes in the zone structures of composites, in particular, the shift of the Fermi level to the right. The growth of the mass fraction of magnetite leads to a noticeable increase in the value of the quantum capacitance at 0 V, from 36.46 F/g for pure graphene to 583.52 F/g in the case of 1:1. Thus, the improvement in the capacity properties of G/Fe₃O₄ composites with increases in the proportion of Fe₃O₄, is mainly caused by significant increases in the Faraday component, due to the participation of Fe₃O₄ in the electrochemical process. These observations may be useful during the design of electrodes for flexible storage devices based on G/Fe₃O₄ composites [7–11,16,17]. The addition of magnetite particles to graphene leads to the appearance of asymmetry in the quantum capacitance of composites. Thus, by varying

the concentration of magnetite, these electrode materials can be used in both hybrid and symmetric supercapacitors [29].

Author Contributions: Conceptualization, V.V.S.; methodology, O.E.G. and V.V.S.; software, O.E.G.; validation, V.V.S. and O.E.G.; formal analysis, O.E.G.; investigation, V.V.S.; resources, O.E.G.; data curation, O.E.G.; writing—original draft preparation, V.V.S.; writing—review and editing, V.V.S., O.E.G.; visualization, V.V.S.; supervision, O.E.G.; project administration, O.E.G.; funding acquisition, V.V.S. and O.E.G. All authors have read and agreed to the published version of the manuscript.

Funding: The research of V.V.S. (conceptualization, methodology, validation, investigation, writing, visualization) was funded by Russian President scholarship, project no. SP-3976.2021.1. O.E.G. (methodology, software, validation, formal analysis, resources, data curation, supervision) wishes to thank the Russian Science Foundation (project #21-73-10091) for financial support of the work.

Institutional Review Board Statement: Not applicable.

Informed Consent Statement: Not applicable.

Data Availability Statement: Not applicable.

Conflicts of Interest: The authors declare no conflict of interest.

References

1. Azhar, A.; Yamauchi, Y.; Allah, A.E.; Allothman, Z.A.; Badjah, A.Y.; Naushad, M.; Habila, M.; Wabaidur, S.; Wang, J.; Zakaria, M.B. Nanoporous Iron Oxide/Carbon Composites through In-Situ Deposition of Prussian Blue Nanoparticles on Graphene Oxide Nanosheets and Subsequent Thermal Treatment for Supercapacitor Applications. *Nanomaterials* **2019**, *9*, 776. [CrossRef]
2. Liu, M.; Nan, H.; Hu, X.; Zhang, W.; Qiao, L.; Zeng, Y.; Tian, H. Graphene decorated iron oxide negative electrodes with high capacity, excellent rate performance, and wide working voltage for aqueous battery-supercapacitor hybrid devices. *J. Alloys Compd.* **2021**, *864*, 158147. [CrossRef]
3. Samuel, J.; Shah, A.; Kumar, D.; Singh, L.R.; Mahato, M. Preparation, characterization and some electrochemical study of waste derived iron Oxide-Carbon nanocomposite. *Mater. Today Proc.* **2021**, in press. [CrossRef]
4. Zhu, W.; Kierzek, K.; Wang, S.; Li, S.; Holze, R.; Chen, X. Improved performance in lithium ion battery of CNT-Fe₃O₄@graphene induced by three-dimensional structured construction. *Colloids Surf. A Physicochem. Eng.* **2021**, *621*, 126014. [CrossRef]
5. Fan, S.; Bresser, D.; Passerini, S. Transition Metal Oxide Anodes for Electrochemical Energy Storage in Lithium- and Sodium-Ion Batteries. *Adv. Energy Mater.* **2019**, *10*, 1902485. [CrossRef]
6. Wu, Q.; Jiang, R.; Mu, L.; Xu, S. Fe₃O₄ anodes for lithium batteries: Production techniques and general applications. *Comptes R. Chim.* **2019**, *22*, 96–102. [CrossRef]
7. Liu, M.; Sun, J. In situ growth of monodisperse Fe₃O₄ nanoparticles on graphene as flexible paper for supercapacitor. *J. Mater. Chem. A* **2014**, *2*, 12068–12074. [CrossRef]
8. Zhao, L.; Gao, M.; Yue, W.; Jiang, Y.; Wang, Y.; Ren, Y.; Hu, F. Sandwich-Structured Graphene-Fe₃O₄@Carbon Nanocomposites for High-Performance Lithium-Ion Batteries. *ACS Appl. Mater. Interfaces* **2015**, *7*, 9709–9715. [CrossRef]
9. Shi, W.; Zhu, J.; Sim, D.H.; Tay, Y.Y.; Lu, Z.; Zhang, X.; Sharma, Y.; Srinivasan, M.; Zhang, H.; Hnga, H.H.; et al. Achieving high specific charge capacitances in Fe₃O₄/reduced graphene oxide nanocomposites. *J. Mater. Chem.* **2011**, *21*, 3422–3427. [CrossRef]
10. Huang, J.-L.; Fan, L.-Q.; Gu, Y.; Geng, C.-L.; Luo, H.; Huang, Y.-F.; Lin, J.-M.; Wu, J.-H. One-step solvothermal synthesis of high-capacity Fe₃O₄/reduced graphene oxide composite for use in Li-ion capacitor. *J. Alloys Compd.* **2019**, *788*, 1119–1126. [CrossRef]
11. Zhang, S.; Li, C.; Zhang, X.; Sun, X.; Wang, K.; Ma, Y. High Performance Lithium-Ion Hybrid Capacitors Employing Fe₃O₄–Graphene Composite Anode and Activated Carbon Cathode. *ACS Appl. Mater. Interfaces* **2017**, *9*, 17136–17144. [CrossRef]
12. Mohan, V.B.; Brown, R.; Jayaraman, K.; Bhattacharyya, D. Characterisation of reduced graphene oxide: Effects of reduction variables on electrical conductivity. *MSEB* **2015**, *193*, 49–60. [CrossRef]
13. Arshad, A.; Iqbal, J.; Ahmad, I.; Israr, M. Graphene/Fe₃O₄ nanocomposite: Interplay between photo-Fenton type reaction, and carbon purity for the removal of methyl orange. *Ceram. Int.* **2018**, *44*, 2643–2648. [CrossRef]
14. Taufik, A.; Saleh, R. The Role of graphene in Fe₃O₄/graphene Composites on the Adsorption of Methylene Blue and Their Kinetic Study. In Proceedings of the IOP Conference Series: Materials Science and Engineering, Sanur-Bali, Indonesia, 19–20 October 2016; Volume 196, p. 012003. [CrossRef]
15. Nene, A.; Takahashi, M.; Somani, P.R.; Aryal, H.R.; Wakita, K.; Umeno, M. Synthesis and characterization of graphene-Fe₃O₄ nanocomposite. *Carbon-Sci. Tech.* **2016**, *8*, 13–24.
16. Eskusson, J.; Rauwel, P.; Nerut, J.; Janes, A. A Hybrid Capacitor Based on Fe₃O₄-Graphene Nanocomposite/Few-Layer Graphene in Different Aqueous Electrolytes. *J. Electrochem. Soc.* **2016**, *163*, A2768–A2775. [CrossRef]
17. Gu, S.; Zhu, A. Graphene nanosheets loaded Fe₃O₄ nanoparticles as a promising anode material for lithium ion batteries. *J. Alloy Compd.* **2020**, *813*, 152160. [CrossRef]

18. Mi, W.; Yang, H.; Cheng, Y.; Chen, G.; Bai, H. Magnetic and electronic properties of Fe₃O₄/graphene heterostructures: First principles perspective. *J. Appl. Phys.* **2013**, *113*, 083711. [[CrossRef](#)]
19. Al-Bagawi, A.H.; Bayoumy, A.M.; Ibrahim, M.A. Molecular modeling analyses for graphene functionalized with Fe₃O₄ and NiO. *Heliyon* **2020**, *6*, e04456. [[CrossRef](#)]
20. Shunaev, V.V.; Slepchenkov, M.M.; Glukhova, O.E. Single-Shell Carbon Nanotubes Covered with Iron Nanoparticles for Ion-Lithium Batteries: Thermodynamic Stability and Charge Transfer. *Top. Catal.* **2018**, *61*, 1716–1720. [[CrossRef](#)]
21. Shunaev, V.V.; Ushakov, A.V.; Glukhova, O.E. Increase of γ -Fe₂O₃/CNT composite quantum capacitance by structural design for performance optimization of electrode materials. *Int. J. Quantum Chem.* **2020**, *120*, e26165. [[CrossRef](#)]
22. Hsieh, C.-T.; Lin, J.-Y.; Mo, C.-Y. Improved storage capacity and rate capability of Fe₃O₄-graphene anodes for lithium-ion batteries. *Electrochim. Acta* **2011**, *58*, 119–124. [[CrossRef](#)]
23. Elstner, M.; Porezag, D.; Jungnickel, G.; Elsner, J.; Haugk, M.; Frauenheim, T. Self-consistent-charge density-functional tight-binding method for simulations of complex materials properties. *Phys. Rev. B* **1998**, *58*, 7260–7268. [[CrossRef](#)]
24. Parr, R.G.; Pearson, R.G. Absolute hardness: Companion parameter to absolute electronegativity. *J. Am. Chem. Soc.* **1983**, *105*, 7512–7516. [[CrossRef](#)]
25. Zheng, G.; Witek, H.A.; Bobadova-Parvanova, P.; Irle, S.; Musaev, D.G.; Prabhakar, R.; Morokuma, K.; Lundberg, M.; Elstner, M.; Kohler, C.; et al. Parameter Calibration of Transition-Metal Elements for the Spin-Polarized Self-Consistent-Charge Density-Functional Tight-Binding (DFTB) Method: Sc, Ti, Fe, Co, and Ni. *J. Chem. Theory Comput.* **2007**, *3*, 1349–1367. [[CrossRef](#)]
26. Mulliken, R.S. Electronic Population Analysis on LCAO-MO Molecular Wave Functions. *J. Chem. Phys.* **1995**, *23*, 1833–1840. [[CrossRef](#)]
27. Wood, B.C.; Ogitsu, T.; Otani, M.; Biener, J. First-Principles-Inspired Design Strategies for Graphene-Based Supercapacitor Electrodes. *J. Phys. Chem. C* **2014**, *118*, 4–15. [[CrossRef](#)]
28. Xu, Q.; Yang, G.; Fan, X.; Zheng, W. Improving the Quantum Capacitance of Graphene-Based Supercapacitors by the Doping and Co-Doping: First-Principles Calculations. *ACS Omega* **2019**, *4*, 13209–13217. [[CrossRef](#)]
29. Kolosov, D.A.; Glukhova, O.E. Boron-Decorated Pillared Graphene as the Basic Element for Supercapacitors: An Ab Initio Study. *Appl. Sci.* **2021**, *11*, 3496. [[CrossRef](#)]